International Journal of Environmental Sciences
ISSN: 2229-7359
Vol. 11 No. 21s, 2025
https://theaspd.com/index.php

In Vitro And In Vivo Evaluation Of Donepezil (DZP) And Curcumin (CUR) Lipid Layered Nanostructured Particle For Brain Damage

Phannideep madala V[1], Somasundaram I[1]
[1]Department of Pharmaceutics, School of Pharmaceutical Sciences, Vels Institute of Science, Technology and Advanced Studies (VISTAS), Pallavaram, Chennai - 600117, Tamil Nadu, India.
*Corresponding author Email Id: somous0926@gmail.com

Abstract
Alzheimer's disease (AD) presents significant challenges due to limited treatment options targeting disease-modifying mechanisms. We developed and characterized nanostructured lipid carriers (NLCs) loaded with donepezil (DZP) and curcumin (CUR) for enhanced AD therapy. These carriers aim to improve drug delivery to the brain by surpassing the blood-brain barrier (BBB) and enhancing drug bioavailability. Differential scanning calorimetry (DSC) analysis confirmed the amorphous state of DZP and CUR loaded NLCs, enhancing drug solubility within the lipid matrix. Scanning electron microscopy (SEM) affirmed the spherical and uniform morphology of the NLCs. In vitro release studies demonstrated sustained drug release profiles with biphasic patterns, indicating surface adsorption and matrix diffusion mechanisms. Higuchi's model best described the release kinetics, suggesting diffusion-controlled drug release from the lipid matrix. Ex vivo permeation studies on sheep nasal mucosa showed efficient drug permeation, indicating the potential of NLCs for nasal drug delivery. The result of in vivo and stability studies support the potential of NLC. These findings suggest promising applications for NLC formulations in AD therapy, warranting further evaluation of their efficacy and safety in in vivo AD models.
Keywords: *Nanostructured lipid carriers (NLCs), Blood-brain barrier (BBB), Differential scanning calorimetry (DSC), Scanning electron microscopy (SEM).*

INTRODUCTION:

The basis of genetic etiology, AD can be classified as familial AD (FAD) and sporadic AD (SAD). The inheritance of AD has been explained by genetic analysis of some rare cases of early onset FAD (1). FAD represents <1% of all AD cases and is caused by mutations in app , ps1 and ps2 genes responsible for expression of APP, presenilin-1 and 2 (PS-1 and PS-2) proteins. They are located on chromosome 21, 14 and 1 respectively (Price and Sisodia, 1998). SAD occurs at >65 years of age and represents 99% of AD cases. In majority of these cases, there were no mutations in genes involved in FAD (2). Olson and co-workers have found a gene on chromosome 20p to be involved in SAD (3,4). Mutations and polymorphism in multiple genes contribute to SAD pathogenesis along with non-genetic factors (5,6). Elevated Aβ levels in brain generate neurotoxic Aβ oligomers which may disrupt normal brain function or aggregate to form plaques which represent a major pathological step in progression of AD. In addition polymorphism in genes for apolipoprotein E (apo E), α-2 microglobulin, very low density lipoprotein receptor and low density lipoprotein receptor-related protein (LRP) are involved in AD pathogenesis (7). Presence of apoE ε4 allele has been linked to increased risk of AD. apoE increases Aβ aggregation in CNS. Patients carrying ε4 allele have minimal inhibitory effect of apoE leading to higher deposition of Aβ (8).

Currently approved drugs for treating the cognitive impairments in AD are based on neurotransmitter or enzyme replacement/modulation. Acetylcholinesterase inhibitors (AChEIs) are the main class of drugs used in AD. Tacrine was the first AChEI approved by the US Food and Drug Administration (FDA) for the treatment of AD. However, it was withdrawn due to side effects like hepatotoxicity. Donepezil (DZP), galantamine and rivastigmine are second generation AChEIs (16)

BACE-2 is a homologue of BACE1 (55% homology) having similar substrate specificity but there is no evidence of it being involved in cleavage of APP and AD pathology. Presenilins PS-1 and PS-2 are catalytic components of γ-secretase (9). Their mutation results in enhanced Aβ42 level and is involved in FAD. They are membrane proteins comprising of 463 and 448 amino acids (10,11,12). Apart from senile plaques, AD is associated with NFT which are intraneuronal aggregates of hyperphosphotylated tau, a microtubule associated protein (MAP). They are found in neurons with trace amounts in non-neuronal

cells. They play an important role in polymerization and stabilization of microtubules and transport of organelles. Tau proteins bind microtubules through microtubule binding domains (13). Hyperphosphorylation of tau causes destabilization of microtubules by aggregation of tau proteins into paired helical filaments, impairs axonal transport and forms NFTs leading to death of neurons. Hyperphosphorylation of tau proteins may be due to increase in kinase activity or decrease in phosphatase activity. Glycogen synthase kinase 3 (GSK 3) is one of the kinases implicated in AD (14). Tau pathology commences in the entorhinal/hippocampal region and spreads into different cortical regions (15).

The present treatment strategies offer primarily symptomatic benefits, providing temporary cognitive improvement and deferred decline with little or no evidence of slowing disease progression (17). AChEIs are associated with gastrointestinal adverse effects like nausea and vomiting that most commonly lead to discontinuation of treatment (18). Alternative routes may provide benefits relative to oral dosing. For instance, the relatively low bioavailability of oral tacrine (19) has generated interest in delivery via various epithelial tissues, including the nasal route (20).

Curcumin (CUR) (diferuloyl methane) is a phenolic phytochemical obtained from rhizome of herb Curcuma longa L commonly known as turmeric (21). Several pre-clinical and molecular studies have been conducted with CUR to evaluate its potential roles as an anti-oxidant and anti-inflammatory. It has been found to exert beneficial effects on experimental models of AD (22).
The two basic paradigms in CNS drug targeting are molecular carrier approach and polymeric carrier approach (23). By the molecular approach drugs can be targeted to brain cells and become activated once inside the target cell by specific enzymes. The disadvantage of this approach is the limited availability of such drugs and the metabolic pathways for potential exploitation. The second major paradigm is by the use of polymeric carriers either administered intravenously, intranasally, intrathecally or as an implantable cerebral device. Among various nanoparticulate drug delivery systems, lipid based nanocarriers viz. solid lipid nanoparticles (SLN), nanostructured lipid carriers (NLC) and nanoemulsion (NE) are increasingly being utilized in pharmaceutical research to encapsulate, protect and deliver bioactive components.
The central composite design (CCD) and Box-Behnken design (BBD) are the most commonly used design for RSM. The BBD has advantage over CCD in that it requires fewer run when the numbers of factors investigated are three. It loses this advantage when number of factor investigated goes to four. It is an independent quadratic design in that it does not contain embedded factorial or fractional factorial design. In this design factor, variable combinations are at the midpoint of edges of the variable space and at the centre. These designs are rotatable and require 3 levels of each factor (24). In CCD, the rotatable characteristic enables to identify the optimum responses around its center point without changing the predicting variance (25). On the other hand, traditional pharmaceutical development of any dosage form involving trial and error methodology is quite time consuming, expensive and laborious. It involves the concept of "changing one variable at a time, while keeping others as constant". This methodology is unpredictable and at times unsuccessful (26). The limitations of traditional formulation and development have paved a way for application of DoE approach in the pharmaceutical industries.

METHODOLOGY:

Differential Scanning Calorimetry (DSC)

The crystalline behavior of both drug and lipid was studied by DSC. Thermograms were recorded for pure drug, lipid and lyophilized drug loaded NLC. DSC was carried out as per the procedure described earlier. Degree of crystallinity of lyophilized drug loaded NLC was calculated by comparing the enthalpy of NLC with enthalpy of bulk lipid (27). The melting enthalpy of bulk lipid was used as a reference (100%) to calculate the percentage of crystallinity of NLC.

$$C\% = \frac{\Delta H_{NLC}}{\Delta H_{bulk}} \times 100$$

where, ΔH_{NLC} indicates enthalpy of freeze dried NLC
ΔH_{bulk} indicates enthalpy of bulk lipid.

Formulation of nanoemulsion

Pseudoternary phase diagrams

The nanoemulsions were prepared using spontaneous nanoemulsification method and phase behavior was studied using pseudoternary phase diagrams (28).

Pseudoternary phase diagrams were constructed using aqueous titration of oil, surfactant and co-surfactant mixture. The oil phase was heated gently at 45-50 °C for 5 min. Surfactant and co-surfactant (smix) were mixed together in different volume ratios (1:0, 1:1, 1:2, 1:3, 2:1, 3:1) and heated at same temperature. These smix ratios were chosen to reflect the increasing concentration of co-surfactant with respect to surfactant and increasing concentration of surfactant with respect to co-surfactant for the detailed study of the phase diagrams for the formulation of NE. Oil and smix were mixed in different volume ratios (1:9, 2:8, 3:7, 4:6, 5:5, 6:4, 7:3, 8:2 and 9:1) to form homogenous isotropic mixtures and were slowly titrated with aqueous phase. The amount of aqueous phase added was at interval of 5% v/v. After each addition of aqueous phase, visual observations were made as clear nanoemulsions, nanoemulsion gels, emulsions or emulsion gels. Oil, surfactants and cosurfactants were grouped in three different combinations for phase studies (Table 1).

Table 1. Oil, surfactants and cosurfactants grouped in different combinations

Group	Oil	Surfactant	Co-surfactant
I	CTX 500+ Capmul MCM	Tween 80	PEG 400
II	CTX 500+ Capmul MCM	Tween 80 + Cremophor EL	PEG 400
III	CTX 500+ Capmul MCM	Tween 80 + Cremophor EL	PEG 400 + Transcutol

Particle /globule size and zeta potential analysis

The mean particle/globule size and ZP of NLC and NE/MNE were determined using a zetasizer ZS 90 (Malvern Instruments, UK). The mean particle/globule size was measured based on photon correlation spectroscopy technique that analyzes the fluctuations in dynamic light scattering due to brownian motion of the particles. The mean diameter was obtained at an angle of 90° in 10 mm diameter cells at 25°C. The ZP, reflecting the electric charge on the particle surface, is a very useful way of evaluating the physical stability of any colloidal system. It was determined based on an electrophoretic light scattering technique (29). All size and ZP measurements were carried out at 25°C using disposable polystyrene cells and disposable plain folded capillary zeta cells, respectively, after appropriate dilution of all samples with original dispersion medium (30). Three replicate analysis was performed for each formulation, and data presented as mean ± S.D.

Drug content

The NE/MNE formulations were diluted to required concentration using acetonitrile as solvent and drug content was estimated using HPLC method. The drug content (N=3) was calculated as:

$$\text{Drug content (\%)} = \frac{\text{Analyzed content}}{\text{Theoretical content}} \times 100$$

Scanning electron microscopy (SEM)

External surface morphology of lyophilized drug loaded NLC was recorded using SEM (FEI QUANTA 200 SEM/EDAX, UK) at 20kV as an accelerating voltage (32). Weighed amount of samples (5-7mg) were mounted on an aluminium stub with double sided adhesive tape. The tape was firmly attached to the stub and lyophilized sample was scattered carefully over its surface. The stub with the sample was then sputter coated with a thin layer of gold to make the sample conductive. Processed sample was subjected to SEM analysis. The images were captured under magnification of 10,000-15,000x and recorded.

In vitro Release Studies:

The release of drug from developed formulations (NLC and NE/MNE) and solution was performed in SNF pH 6.4 containing 1% SLS using the dialysis bag method (34). For both the drugs, solution was

prepared by dissolving 80 mg of DZP and 120 mg of CUR in a mixture of 1mL ethanol and 2mL propylene glycol and finally volume was made to 10mL with distilled water separately to produce concentration of 8mg/mL for DZP and 12mg/mL for CUR. Dialysis membrane having pore size of 2.4nm and molecular weight cut off 12,000-14,000 (Dialysis membrane-150, HiMedia, Mumbai, India) was used. The bags were soaked in distilled water for 24h before use. Drug solution, lyophilized drug loaded NLC and drug loaded NE/MNE were placed in dialysis bags separately and sealed at both the ends. The bags were placed in baskets (USP Dissolution apparatus Type I, Lab India, Mumbai) and immersed in 500mL of dissolution medium maintained at 37±0.5°C and stirred at 100rpm. Aliquots of the samples were withdrawn from dissolution medium at regular time intervals and same volume of fresh dissolution medium was replaced to maintain a constant volume. The samples were analyzed for drug content by HPLC (n=3). The drug release profile was constructed by plotting the cumulative percent drug release versus time (h). The kinetic analysis of the release data were fitted to various kinetic models such as zero order, first order and Higuchi's equation (35).

Ex vivo Permeation Studies:

To investigate the permeation efficacy of drug from NLC, NE/MNE and solution across the freshly excised sheep nasal mucosa, ex vivo permeation studies were performed using the Franz diffusion cell with surface area of 1.79cm^2 and volume of 25mL (Kovai Glass Works, Coimbatore, India) (36). The freshly excised sheep nasal mucosa was collected from the slaughter house in PBS, pH 6.4. Excised superior nasal membrane was cut to an appropriate size and thickness (0.2mm), made free from adhered tissues and mounted between the donor and receptor compartment of the Franz diffusion cell, with mucosal side facing the donor compartment. The mounted tissue was allowed to stabilize and stirred under SNF pH 6.4 containing 1% SLS (diffusion medium) for 15min on a magnetic stirrer. The diffusion cell was thermostated at 37±0.5°C. Solution from both the compartments was removed after 15min, and the receptor compartment was freshly filled with diffusion medium. The mounting of nasal membrane was done on the rim of the receptor compartment; the donor compartment of diffusion cell was placed over it and secured with a clamp to avoid the leakage of diffusion media. Permeation studies of pure drug solution, lyophilized drug loaded NLC reconstituted with SNF and drug loaded NE/MNE were carried out by placing 1mL onto stabilized sheep nasal membrane on donor compartment and continuously magnetic stirred at 600rpm. Aliquot (0.5mL) of media were withdrawn from the receptor compartment at predetermined time intervals, filtered through 0.45µm nylon filter paper and analyzed for drug content using HPLC. Each removed sample was replaced immediately by an equal volume of fresh diffusion media maintained at 37±0.5°C to maintain the constant volume at each time interval. Each study was carried out for a period of 6h, during which the amount of drug permeated across the sheep nasal mucosal membrane was determined at each sampling point using HPLC (n=3). The permeation profile was constructed by plotting the amount of drug permeated per unit skin surface area (µg/cm^2) versus time (h). The steady state flux (J_{ss}, µg /cm^2.h) was calculated from slope of the plot using linear regression analysis. The kinetic analysis of the release data were fitted to various kinetic models such as zero order, first order and Higuchi's equation (37).

In vitro cytotoxicity assay

The toxicity studies of the blank and drug loaded formulations (NE/MNE and NLC) were carried out in SK-N-SH cells, a human neuroblastoma cell line. The cells were maintained in minimum essential medium (MEM), supplemented with 10% v/v FBS, penicillin (100 IU/mL), streptomycin (100 g/mL) and amphotericin B (5 •g/mL) in a humidified atmosphere of 5% CO_2 at 37°C until confluent. The cells were then seeded in multiwall culture plates for experimental procedure. The cytotoxicity assay was carried out using cell suspension, containing 5,000 cells seeded in each well of a 96 well microtiter plate (Nunc and Tarsons, Kolkata, India) and incubated for 24h at 37°C. Cells were treated with 250-2,000 •g/mL concentration of nanoformulations. Control cells were incubated without the test compound and with MEM. The microtiter plates were incubated at 37°C in a humidified incubator with 5% CO_2 for a period of 72h. Morphological changes in the cells were inspected daily and observed for microscopically detectable alterations, i.e., loss of monolayer, granulation and vaculation in the cytoplasm. The cytopathic effect was observed. A plot of % growth inhibition versus concentration was plotted to determine the IC_{50} value (Concentration of the drug that produces 50% inhibition of the cells) by SRB (Sulphorhodamine B) assay (Skehan et al., 1990).

In vitro hemolytic toxicity

The hemolytic activity has been suggested as a toxicity screen in vitro and it also serves as a simple and reliable measure for estimating the membrane damage caused by formulation in vivo. The in vitro hemolytic potential of the formulations was studied by using the method proposed by Jumaa et al. (Jumaa et al., 1999). The Fresh blood from rats was collected in a vial containing ethylene diamine tetraacetic acid (EDTA) as an anticoagulant. Blood was centrifuged at 3000rpm for 20min to remove white blood cells (WBC) debris and suspended RBCs were taken out. The RBCs were washed 3 times with isotonic saline solution (0.15M NaCl and pH 7.4) before diluting with buffer to prepare erythrocyte stock dispersion. The RBC cell suspension was adjusted to 50% hematocrit. Hemolysis experiments were carried out for both blank and drug loaded formulations of NE and NLC at a concentration of 0, 5, 10, 25, 50, 100, 250 and 500•g/mL. Incubation was carried at 37°C for a period of 1h. After incubation under shaking, debris and intact RBCs was removed by centrifugation and 100µL of resulting supernatant was dissolved in 2mL of an ethanol/hydrochloric acid (HCl) mixture (39:1, 99% ethanol and HCl, w/v). This mixture dissolves all components and avoids the precipitation of hemoglobin. The absorbance of the mixture was determined at 398nm by spectrophotometer monitoring against a blank sample. Control sample of 0% lysis (in buffer) and 100% lysis (in Triton X 100) was employed in the experiment. The % hemolysis caused by the test sample (n=3) was calculated by following equation:

$$\% \text{ Hemolysis} = \frac{\text{Absorbance of Test - Absorbance at 0\%}}{\text{Absorbance at 100\% lysis - Absorbance at 0\%}} \times 100$$

Nasal ciliotoxicity studies on sheep nasal mucosa

Nasal ciliotoxicity studies were carried out using the freshly isolated sheep nasal mucosa collected from a slaughter house in a phosphate buffered saline (PBS) pH 6.4 (Seju et al., 2011). Each piece was treated with drug solution in PBS pH 6.4, blank NLC, lyophilized drug loaded NLC, blank NE, drug loaded NE/MNE, PBS pH 6.4 (as negative control) and isopropyl alcohol (IPA) (nasal mucociliary toxicity agent used as a positive control), respectively. After treatment for 2h, all the samples were washed properly with distilled water and were preserved with 10% formalin until further analysis. Each sample was sectioned and stained with H and E. The mucosa was then dissected out, and the mucocilia was examined on an optical microscope by a pathologist.

Stability studies

The optimized batch of lyophilized drug loaded NLC and drug loaded NE/MNE were evaluated for long term stability for 6 months at 4±1°C and 25±1°C (n=3). Samples were transferred in amber colored glass vials, sealed and were stored upright. NE/MNE formulations samples were withdrawn at specified time intervals (0, 1, 3 and 6 months of storage) and assessed for any change in GS, ZP, refractive index, drug content, viscosity and pH in addition to physical appearance (clarity and phase separation). The clarity and phase separation of the NE/MNE formulations were determined by visual examination under light alternatively against white and black backgrounds. NLC formulations were rehydrated with ultrapure water and evaluated for any change in PS, ZP, DL and EE at specified time intervals (0, 1, 3 and 6 months of storage). Further, polymorphic transition of lipid in NLC formulations upon storage at 25±1°C was assessed using DSC and thermograms were recorded at 0 and 6 months.

RESULT AND DISCUSION

Differential Scanning Calorimetry (DSC)

DSC is a tool to investigate the melting temperature and recrystallization behavior of crystalline material. DSC thermograms were recorded for pure drugs (DZP and CUR), lipid (TP), and lyophilized NLC (CNLC and DNLC). The DSC curve of DZP and CUR showed a single sharp endothermic peak at 228.91 and 183.07 °C respectively. The thermograms of DZP and CUR loaded NLC did not show the melting peak of respective drugs. This suggests that drugs were not in crystalline state but amorphous state. Since, NLC were prepared by rapid quenching of microemulsion, drug molecules dispersed in lipid phase are not able to crystallize (36). Furthermore, the presence of surfactants inhibits crystallization of the drug. Degree of crystallinity of lyophilized NLC was calculated by comparing the enthalpy of NLC with enthalpy of bulk lipid (Freitas and Müller, 1999). The melting enthalpy of bulk lipid was used as a reference (100%) to calculate the percentage of crystallinity of NLC. DNLC and CNLC showed percent crystallinity of 14.77 and 16.17% (Table 2).

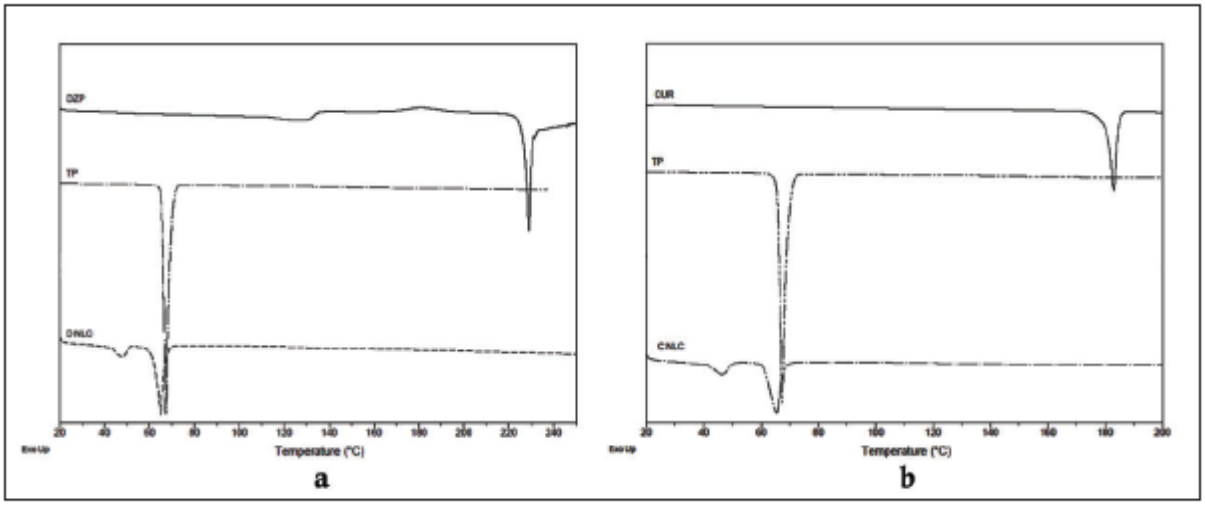

Fig.1. Overlaid DSC Thermogram of (a) Donepezil NLC (b) Curcumin NLC

The endothermic peak of bulk lipid TP (67.29°C) was found to shift to 65.14 and 65.34°C in DNLC and CNLC respectively. This could be attributed to presence of liquid lipid and drug in NLC matrix. This supports that the oil is moleculary dispersed in the lipid blend, which creates distortation in the lipid matrix (37). The peak height and enthalpy of lipid was further reduced in NLCs. Thus reduction in crystallinity was observed for both drug and lipid matrix (less solid lipid crystals) after formulating them as NLCs.

Table 2. Crystallization index of curcumin and donepezil NLC

Lipid	Parameter	Bulk	CNLC	DNLC
Tripalmitin (TP)	Melting peak (°C)	67.29	65.34	65.14
	Enthalpy (J/g)	242.1	109.2	128.33
	Crystallinity (%)	100	14.77	16.17

For large production of NLC, the control of polymorphism is a demand due to its influence on EE and drug expulsion during storage. The lipid polymorphism is also an important characteristic, since the crystalline structures of long chain compounds such as triglycerides can occur in different polymorphic forms (α, β, β) (37). In general, these lipids crystallize in two or three different phases, α and β, or α, β and β2, respectively (Freitas and Müller, 1999). This phenomenon is due to the numerous possible lateral packing patterns of fatty acid chains in a particular organization of hydrocarbon chains (38). The α-form (hexagonal) is the least stable with a lower melting point and latent heat, whereas the β-form (triclinic) is the most stable with higher melting point and higher latent heat. The transformation of α to β (orthorhombic) and β is irreversible and occurs towards a more hydrodynamic stable system (39). The onset of melting and melting points of lipid in NLC formulation were depressed when compared to melting points of corresponding bulk lipid. This indicates that lipid in the formulation might be in the β-polymorphic form (stable modification). This melting point depression and broadening peaks were observed when transforming a bulk lipid into NLC form due to Gibbs-Thompson effect, i.e. the larger ratio of specific surface area to volume of particle with a smaller size when compared to bulk material (Perez, 2005) and/ or the presence of surfactants (40). Depending on the lipophilicity, the surfactants partition between water phase, interface and the lipid phase. Surfactant in the lipid phase can distort crystallization and result in a lower melting enthalpy and lowering of the melting temperature. Further, a shoulder peak of TP was observed in DNLC and CNLC at 47.82 and 46.47°C respectively. This may be attributed to β-polymorphic form (thermodynamically unstable modification) of TP and also due to

presence of liquid lipid (oil) in NLC which suppresses the recrystallization of solid lipid during cooling phase of preparation. The β-polymorph will convert progressively into the stable β-form during the storage (41).

Effect of lipid concentration

It was observed that PS and PDI of lipid nanoparticles was in range of 115.8-334.6 nm and 0.189-0.452 respectively (Table 3). It is obvious that with increase in lipid concentration there was increase in PS. The possible reason might be that amount of lipid was high compared to concentration of surfactant used. In other words, surfactant concentration was not sufficient enough to effectively cover the lipid microemulsion droplets and thus reduce the surface tension. Hence, the droplet size of emulsion was higher and formed large particles when poured into ice cold water. At 2% w/v of lipid concentration PS was significantly higher with large PDI. Hence, it is clear that lipid nanoparticles having size <200 nm with low PDI can be prepared at concentration ≤ 1.5 % w/v.

Table 3. Influence of lipid concentration on particle size and polydispersity index of lipid nanoparticles

Lipid concentration (% w/v)	Particle size (nm)	Polydispersity (PDI)
0.5	115.8±12.7	0.189±0.021
1.0	183.7±8.7	0.254±0.032
1.5	198.4±15.7	0.232±0.024
2.0	334.6±13.5	0.452±0.038

Effect of type of surfactant

It was observed that PS and PDI of lipid nanoparticles prepared with different surfactants was in range of 185.8-1570.2 nm and 0.184-0.778 respectively (Table 4). Among different surfactants smallest PS (196.2±13.5) was obtained with Pluronic F68 with low PDI (0.184±0.017) thus showing superior ability to stabilize the system compared to other surfactants. Although, HLB values of surfactants used in study were >10, there were considerable differences in their ability to emulsify the lipid matrix. Results indicated that apart from HLB value, other factors like structure and relative hydrophobic chain lengths of surfactants had influence on nanosization. Cremophor EL is a bulkier surfactant possessing polyethylene glycols and glycerol ethoxylates of long chain ricinoleic acid. This could have imparted poor stabilizing efficiency leading to large PS (1570.2±64.3 nm). On the contrary, Tween 20 and Tween 80 by virtue of tetrahydrofuran ring with polyoxyethylene chains might have imparted greater surface coverage of NLC and enabled smaller PS (Strickley, 2004). Pluronic F68 is a large molecular weight nonionic block copolymer of polyoxyethylene oxide (hydrophilic segment) and polyoxypropylene oxide (hydrophobic segment) (42,43). This polyoxypropylene oxide (hydrophobic segment) accommodates at interface and dense polymeric network of polyoxyethylene oxide (hydrophilic segment) orients in external phase causing steric stabilization of lipid nanoparticles. This mutual hydrophilic/hydrophobic interaction with lipid nanoparticles provides sufficient steric hindrance to inhibit the particle growth.

Table 4. Influence of type of surfactant on particle size and polydispersity index of lipid nanoparticles

Surfactant	Particle size (nm)	Polydispersity (PDI)
Tween 20	224.9±16.1	0.238±0.027
Tween 80	205.8±7.5	0.176±0.021
Cremophor EL	1570.2±64.3	0.778±0.097
Pluronic F68	196.2±13.5	0.184±0.017
Pluronic F127	216.8±18.3	0.303±0.032

Scanning electron microscopy (SEM)

The external morphological studies using scanning electron microscope (SEM) revealed that the particles were round and homogeneous with smooth surface and fixed in the bulk and grid structure formed by cryoprotectants (Fig. 2). There was no drug crystal or aggregation of particles visible in the graph. The lyophilized powder could be re-dispersed in water easily. This would be helpful for the reconstitution of the dry powder and stability during storage. The nanoparticle size observed by SEM correlated well with the PS measured by particle size analyzer.

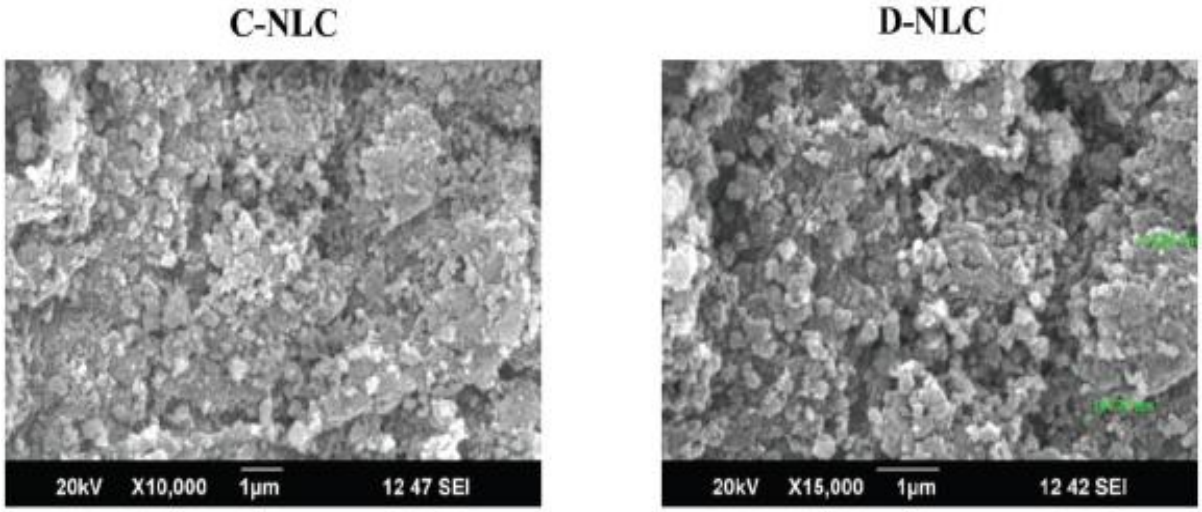

Fig. 2. SEM morphology of curcumin NLC (CNLC) and donepezil NLC (DNLC), showing the surface structure of the lyophilized powder

In vitro release studies

The release of drugs (DZP and CUR) from NLCs was significantly lower compared to pure drug solutions. The results are shown in Fig. 4. The release of DZP from drug solution (DS) was significantly higher ($p < 0.001$) than DNLC. DS showed 97.82 ± 2.75% release at the end of 24h whereas only 22.70 ± 1.61% of drug was released from DNLC. Similar trend was observed in release behavior of CUR from NLC formulation. The release of drug from solution (CS) was significantly higher ($p < 0.001$) than CNLC. CS showed 78.71 ± 1.16% release at end of 72 h compared to 30.55 ± 0.94% for CNLC.

The slower release of CUR from solution in comparison to DZP may be due to limited solubility of CUR in dissolution media (1.733±0.251) compared to high solubility of DZP (21.37±1.688 mg/mL).

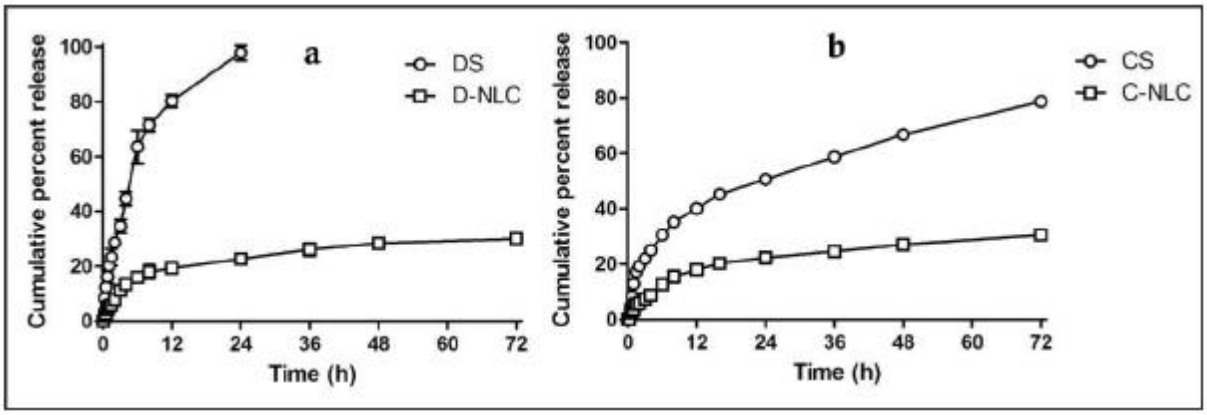

Fig. 4. In vitro release profile of donepezil NLC (DNLC) and curcumin NLC (CNLC) in comparison with respective drug solutions

Both DNLC and CNLC showed biphasic release pattern i.e. an initial faster release followed by sustained release. In first 8h, 18.00 ± 2.51% and 15.50 ± 3.06% of drug was released from DNLC and CNLC respectively followed by release upto 72h (~30%). The initial occurrence of faster release from both NLC formulations clearly indicate the location of a certain amount of drug adsorbed onto the surface of NLC or precipitated from the superficial lipid matrix. This can also be explained by inhomogeneity of oil in

inner lipid matrix. The difference in melting behaviour of liquid and solid lipid leads to accumulation of oil in outer shell of NLC resulting in faster release of drug in initial stages (44,45). The liquid lipid enriched shell possesses higher solubility for lipophilic drugs and they could be released by diffusion or erosion of matrix (46). Subsequent sustained release of the drug suggests the diffusion of drugs from the core of the lipid matrix to the release medium (35). Slow release of DZP and CUR from NLC suggests that the drugs are homogenously dispersed in lipids matrix. Further, solid lipid matrix has higher viscosity thus slowing down the release according to Stokes-Einstein's law (38). The drug release data obtained were fitted into release kinetic model: zero order, first order and Higuchi's equation. Release of drug from NLC followed Higuchimodel better than other equations and was found to be diffusion controlled from homogenous and granular matrix systems. The drug release from a matrix system is said to follow Higuchi's release kinetics if the amount of drug released is directly proportional to the square root of time.

Table 6. Dissolution model studies by fitting dissolution data of curcumin and donepezil nanostructured lipid carriers

Model	Equation	Formulations	R^2 value
Zero order	m_o-m=kt	CS	0.837
		CNLC	0.787
		DS	0.937
		DNLC	0.734
First order	ln m=kt	CS	0.902
		CNLC	0.817
		DS	0.986
		DNLC	0.772
Higuchi's model	m_o-m=$kt^{1/2}$	CS	0.964
		CNLC	0.953
		DS	0.984
		DNLC	0.920

In vitro hemolytic toxicity

The nanoparticles may be transported to systemic circulation upon intranasal administration and can cause damage to RBCs. To assess the safety of the developed formulations in vitro hemolytic toxicity studies were carried out by incubating isolated RBC cells with the blank and drug loaded nanoformulations (NE/MNE and NLC). The results revealed (Table 7) that both the blank and drug loaded nanoformulations tested at concentration range of 0-500µg/mL in PBS showed negligible hemolytic effect (0.17-2.15%) and was within acceptable range (<5%) (Mocan, 2013). Triton X 100, a known hemolytic agent acted as a positive control in the study and showed 100% hemolysis of RBCs; thus validating the experiment. It should also be noted that the observations of the in vitro hemolytic study do not exactly predict the in vivo behavior but it gives some idea about the hemolytic potential. Also, in the present study, test samples were contacted with RBCs for 1h which is unlikely to happen in vivo. Therefore, the estimated in vitro RBCs toxicity may be largely reduced in vivo.

Table 7 In vitro hemolytic assay of nanoformulations

Conc (µg/mL)	Percent hemolysis (%)							
	BLANK	CNLC	DNLC	BLANK	CNE	DNE	CMNE	DMNE

	NLC			NE				
5	0.17±0.02	0.19±0.03	0.18±0.01	0.50±0.11	0.53±0.08	0.51±0.03	0.51±0.06	0.48±0.05
10	0.19±0.04	0.20±0.02	0.19±0.03	0.82±0.23	0.84±0.13	0.82±0.15	0.82±0.09	0.75±0.07
25	0.23±0.04	0.24±0.03	0.22±0.03	1.01±0.12	1.11±0.07	1.05±0.13	1.09±0.11	0.99±0.08
50	0.26±0.07	0.27±0.08	0.24±0.04	1.20±0.15	1.22±0.11	1.21±0.11	1.20±0.14	1.15±0.10
100	0.25±0.08	0.28±0.03	0.26±0.04	1.39±0.21	1.45±0.15	1.39±0.17	1.42±0.15	1.26±0.12
250	0.33±0.04	0.31±0.04	0.32±0.02	1.71±0.14	1.91±0.12	1.75±0.17	1.89±0.09	1.65±0.15
500	0.46±0.12	0.42±0.07	0.45±0.04	1.97±0.28	2.15±0.18	1.98±0.17	2.03±0.12	1.86±0.18

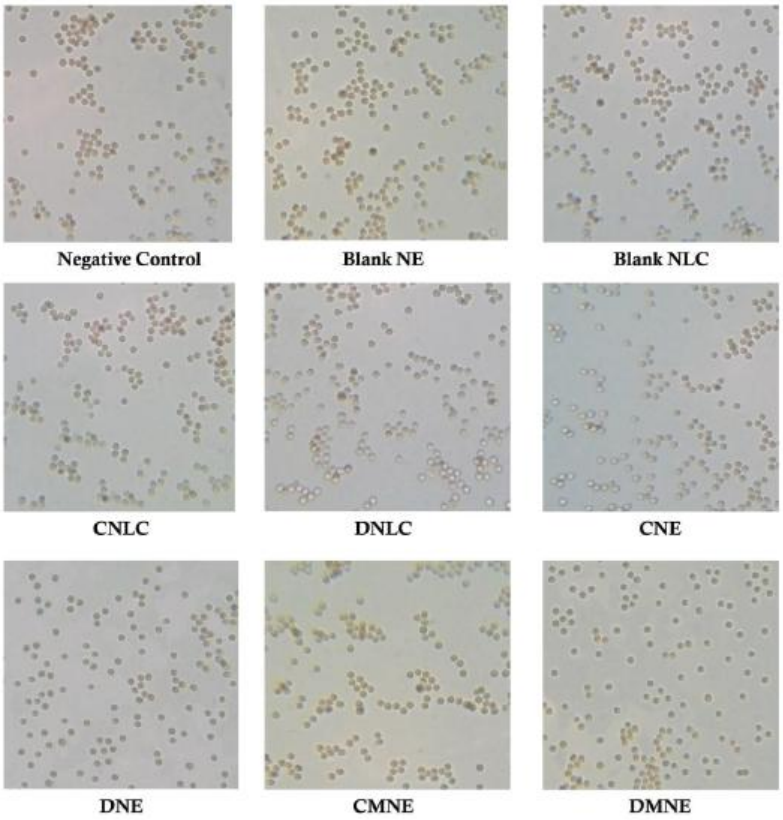

Fig. 5. Visual observations of RBC treated with various nanoformulations under optical microscope (400x)

Nasal ciliotoxicity studies

Nasal ciliotoxicity studies are useful to study the toxicity of excipients used in a formulation. As shown in Fig. 6, nasal mucosa treated with PBS pH 6.4 showed no nasociliary damage and epithelial layer was

intact. Treatment with IPA caused extensive damage to nasal mucosa with loss of epithelial cells, loss of cilia and shrinkage of mucosal layer. Treatment with blank and drug loaded NE/MNE and NLC formulations showed no toxicity on nasal mucosa, thus the excipients used for formulation were safe for nasal administration.

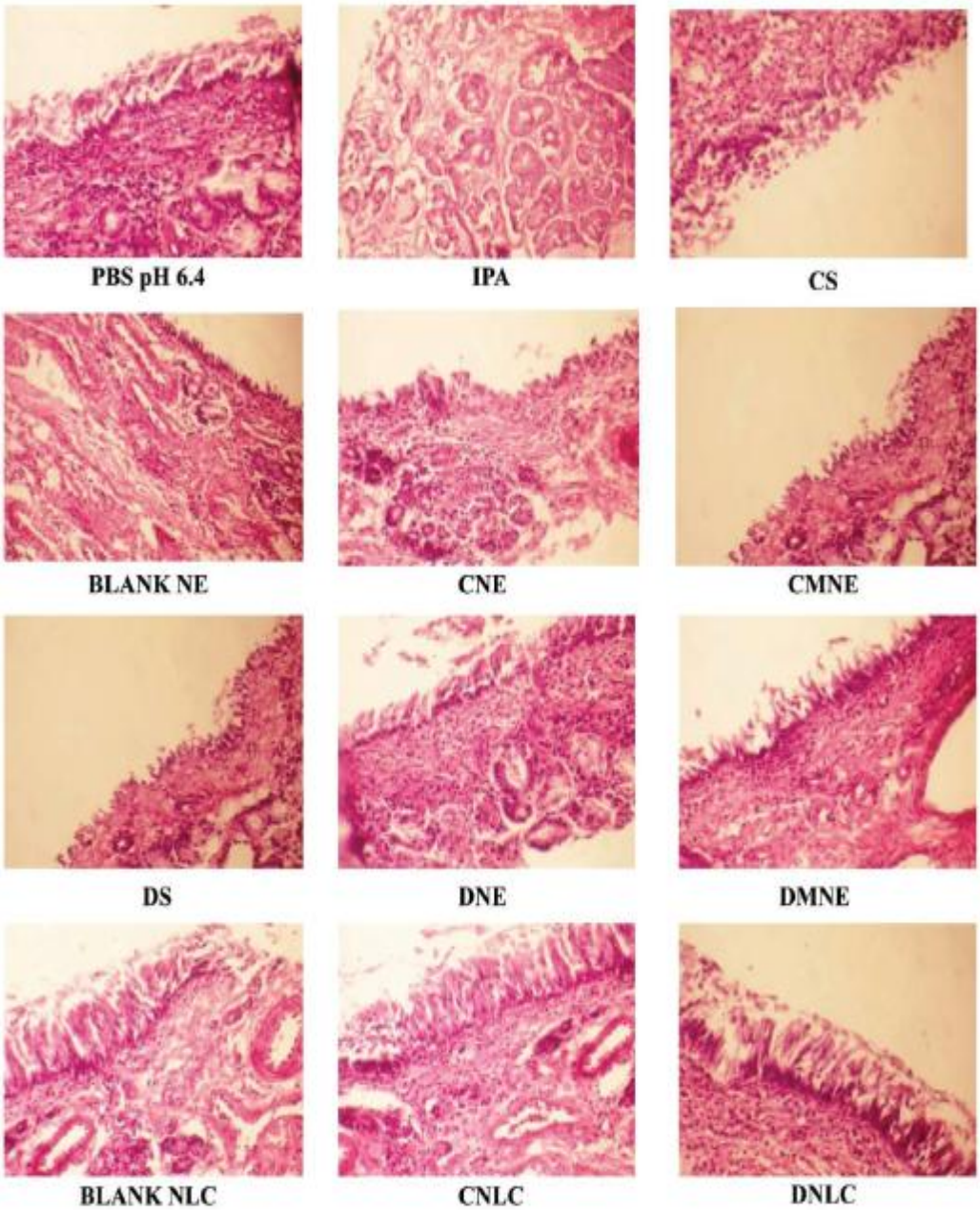

Fig.7. Histopathological sections of sheep nasal mucosa treated with PBS PH 6.4, IPA, curcumin solution (CS), blank nanoemulsion (NE), curcumin nanoemulsion (CNE), curcumin mucoadhesive nanoemulsion (CMNE), donepezil solution (DS), donepezil nanoemulsion (CNE), donepezil mucoadhesive nanoemulsion (CMNE), blank nanostructured lipid carrier (NLC), curcumin NLC (CNLC) and donepezil NLC (DNLC) at magnification of 400x.

Stability studies

The stability studies of drug loaded NE/MNE and NLC were carried out upto 6 months at storage temperature of 4±1°C and 25±1°C. The results indicate both DZP and CUR loaded NE/MNE were stable w.r.t. GS, ZP, refractive index, drug content, viscosity and pH and there was no significant difference ($p>0.05$) at different time periods. Thus, the NE/MNEs were highly stable and were not affected by change in storage temperature. The results are shown in Table 8-11.

Table 8. Storage stability studies of curcumin nanoemulsion

Temperature (°C)	Parameters	Storage Time (months)			
		0	1	3	6
4°C	Globule size (nm)	35.8±2.6	35.7±2.9	35.7±2.8	35.6±3.4
	Zeta potential(mV)	-19.6±1.9	-19.4±2.1	-19.5±1.8	-19.4±1.7
	Refractive index	1.339±0.008	1.340±0.009	1.340±0.008	1.340±0.010
	Drug content (%)	99.71±0.32	99.64±0.41	99.58±0.39	99.14±0.27
	Viscosity (cP)	196.4±5.1	197.8±4.1	197.42±2.9	198.4±1.6
	pH	5.12±0.06	5.11±0.04	5.12±0.07	5.10±0.05
25°C	Globule size (nm)	35.8±2.6	35.9±3.1	37.8±3.4	37.9±3.6
	Zeta potential(mV)	-19.6±1.9	-19.3±1.8	-19.3±2.4	-19.1±2.5
	Refractive index	1.339±0.008	1.339±0.009	1.340±0.005	1.341±0.008
	Drug content (%)	99.71±0.32	99.41±0.29	99.23±0.18	98.62±0.31
	Viscosity (cP)	196.4±5.1	196.8±2.9	196.9±3.1	194.4±2.9
	pH	5.12±0.06	5.13±0.05	5.14±0.04	5.14±0.05

Table 9. Storage stability studies of curcumin mucoadhesive nanoemulsion

Temperature (°C)	Parameters	Storage Time (months)			
		0	1	3	6
4°C	Globule size (nm)	37.8±3.1	37.9±2.8	37.9±2.3	39.4±3.5
	Zeta potential(mV)	27.2±2.1	27.0±2.9	26.8±1.9	26.4±1.7
	Refractive index	1.351±0.004	1.350±0.008	1.350±0.009	1.351±0.010
	Drug content (%)	99.88±0.19	99.75±0.35	99.74±0.39	99.58±0.59
	Viscosity (cP)	233.5±1.9	234.6±2.9	234.9±3.1	236.5±2.8
	pH	5.46±0.04	5.44±0.05	5.45±0.05	5.44±0.06
25°C	Globule size (nm)	37.8±3.1	37.8±3.2	37.9±3.4	41.6±4.1
	Zeta potential(mV)	27.2±2.1	27.4±3.1	26.8±3.5	29.2±3.6
	Refractive index	1.351±0.004	1.352±0.009	1.351±0.011	1.352±0.013
	Drug content (%)	99.88±0.19	99.64±0.23	98.45±0.54	98.14±0.63
	Viscosity (cP)	233.5±1.9	234.1±2.1	234.5±3.9	236.9±3.1
	pH	5.46±0.04	5.45±0.03	5.45±0.04	5.46±0.05

Table 10. Storage stability studies of donepezil nanoemulsion

Temperature (°C)	Parameters	Storage Time (months)			
		0	1	3	6
4°C	Globule size (nm)	32.3±1.2	32.4±2.1	32.9±1.8	33.5±1.8
	Zeta potential(mV)	-22.9±2.1	-22.7±1.8	-22.9±1.4	-22.1±1.8
	Refractive index	1.339±0.006	1.339±0.009	1.340±0.008	1.340±0.009
	Drug content (%)	99.91±0.09	99.90±0.10	99.89±0.13	99.63±0.21
	Viscosity (cP)	195.9±5.1	196.4±3.2	196.8±2.9	197.5±3.6
	pH	5.23±0.09	5.24±0.05	5.23±0.06	5.21±0.06
25°C	Globule size (nm)	32.3±1.2	32.5±2.9	33.8±3.1	35.6±3.8
	Zeta potential(mV)	-22.9±2.1	-21.9±2.9	-20.4±1.9	-18.4±2.1
	Refractive index	1.339±0.006	1.339±0.009	1.341±0.023	1.343±0.008
	Drug content (%)	99.91±0.09	99.12±0.53	99.14±0.23	99.03±0.60
	Viscosity (cP)	195.9±5.1	196.2±2.1	196.9±3.1	195.4±3.6
	pH	5.23±0.09	5.23±0.06	5.22±0.05	5.22±0.06

Table 11. Storage stability studies of donepezil mucoadhesive nanoemulsion

Temperature (°C)	Parameters	Storage Time (months)			
		0	1	3	6
4°C	Globule size (nm)	39.8±1.8	40.4±2.9	42.1±3.1	43.4±1.7
	Zeta potential (mV)	26.2±1.6	26.0±1.8	25.4±1.9	22.9±2.3
	Refractive index	1.352±0.004	1.352±0.005	1.353±0.004	1.358±0.009
	Drug content (%)	99.45±0.54	99.39±0.45	99.20±0.56	98.54±0.46
	Viscosity (cP)	234.6±3.6	235.1±2.9	236.1±3.1	237.8±3.4
	pH	5.61±0.05	5.57±0.04	5.58±0.07	5.54±0.04
25°C	Globule size (nm)	39.8±1.8	42.5±2.3	43.2.±3.1	45.4±2.9
	Zeta potential (mV)	26.2±1.6	24.9±2.9	23.6±2.4	22.1±1.9
	Refractive index	1.352±0.004	1.352±0.006	1.33±0.005	1.353±0.006
	Drug content (%)	99.45±0.54	99.42±0.33	99.21±0.41	99.16±0.29
	Viscosity (cP)	234.6±3.6	235.4±2.7	234.9±3.6	235.9±4.1
	pH	5.61±0.05	5.59±0.07	5.59±0.05	5.55±0.07

Table 12.Storage stability studies of curcumin and donepezil NLC formulations

Formulation	Temp.	Parameters	Storage Time (months)			
			0	1	3	6
CNLC	4°C	Particle size (nm)	130.4±8.9	131.2±7.6	133.4±5.6	136.4±6.1
		Zeta potential (mV)	-38.2±2.1	-37.4±2.9	-36.2±1.8	-34.1±1.4
		Drug loading (%)	14.41±0.37	14.39±0.42	14.39±0.38	14.34±0.62
		Entrapment efficiency (%)	94.29±1.20	94.11±0.74	94.11±0.48	93.78±0.75
	25°C	Particle size (nm)	130.4±8.9	132.8±7.5	135.4±6.6	156.9±6.4**
		Zeta potential (mV)	-38.2±2.1	-37.1±1.8	-35.2±1.4	-31.4±2.1**
		Drug loading (%)	14.41±0.37	14.38±0.43	14.18±0.23	13.91±0.87
		Entrapment efficiency (%)	94.29±1.20	94.04±0.81	92.73±0.91	91.97±1.68
	4°C	Particle size (nm)	134.4±8.5	135.1±6.3	138.9±6.6	143.7±6.9
		Zeta potential (mV)	-32.4±2.9	-32.1±1.8	-31.8±2.3	-29.5±1.2
		Drug loading (%)	14.89±1.07	14.88±0.63	14.87±0.83	14.86±0.39

DNLC		Entrapment efficiency (%)	93.29±1.31	93.14±0.89	93.08±0.67	93.02±0.47
	25°C	Particle size (nm)	134.4±8.5	139.4±4.6	146.6±5.6*	159.7±9.6**
		Zeta potential (mV)	-32.4±2.9	-31.4±1.6	-29.4±1.7	-26.4±1.9*
		Drug loading (%)	14.89±1.07	14.87±0.43	14.78±0.46	14.76±0.34
		Entrapment efficiency (%)	93.29±1.31	93.08±0.87	92.52±0.69	92.08±0.44

Significant * (p<0.05); **(p<0.01); ***(p<0.001) in comparison to Day '0'

However, in case of NLCs there was significant (p<0.01) increase in PS when stored at 25°C in comparison to 4°C. The results are given in Table 12. The PS of CNLC increased from 130.4±8.9 to 156.9±6.4 nm at 25°C. Similarly, PS of DNLC increased from 134.4±8.5 to 159.7±9.6 nm at 25°C. However, it was still in nano-range and optimal for nasal delivery. In contrast, the PS growth was slower (p>0.05) when NLC were stored at 4°C. The high temperature (25°C) increased the kinetic energy of system, which could accelerate the collision of particles, and consequently increased the possibility of aggregation for nanoparticles (Freitas and Müller, 1998; Hu et al., 2006). The ZP of NLCs was decreased upon storage and was more pronounced at higher temperature. The increased energy input at higher temperature can lead to changes in crystalline structure of the lipid. Crystalline re-orientation can result in changes of the charges on the particle surface (Nernst potential) and subsequently measured ZP. In addition, different sides of crystal can possess a different charge density and during one-dimensional growth of crystal the surface ratio of differently charged crystal side changes and consequently the measured ZP changes. According to the DLVO theory, a system can be regarded as stable if the electrostatic repulsion dominates the attractive van der Waals forces. The particles have to overcome an energy barrier of electrostatic repulsion to approach closely and form agglomerates. If their velocity or kinetic energy is high enough they will collide. Higher temperatures increase the kinetic energy of a system, in combination with a reduced ZP this leads to aggregation of nanoparticles (Freitas and Müller, 1998).

The DL and EE of CNLC and DNLC was decreased upon storage but it was statistically non-significant (p>0.05). The lipids undergo polymorphic transitions upon storage which may result in drug expulsion. NLC formulations have advantage of having low crystallanity compared to SLN leading to better storage stability. The results indicate that developed NLC were very stable. Based on the results obtained it can be concluded that developed NLC formulations were more stable at 4°C compared to 25°C.

To further investigate the storage stability of NLC formulations, DSC studies were carried out at 0 and 6 months. The results are shown in Fig. 60. As evident from the results obtained there was no change in the melting point of the lipid even after 6 months of storage. However, the melting point of shoulder peak was shifted in both DNLC and CNLC. The melting point of shoulder peak in DNLC was shifted from 42.5 to 49.7°C and in case of CNLC it was shifted from 46.4 to 43.5°C. As discussed earlier, these shoulder peaks are attributed to α-polymorphic form of the lipid, which is less stable and has lower point. Upon storage lipids undergo transition from α to β and β form which is responsible for shift in melting point of shoulder peak.

CONCLUSION:

The work focuses on the creation and characterisation of nanostructured lipid carriers (NLCs) loaded with donepezil (DZP) and curcumin (CUR) to improve medication delivery in Alzheimer's disease (AD) therapy. The amorphous condition of DZP and CUR loaded NLCs was validated by DSC measurement, which improved drug solubility in the lipid matrix. The consistent morphology was confirmed by

transmission electron microscopy and scanning electron microscopy. Biphasic patterns of prolonged drug release were seen in in vitro release investigations. Hence the formulation to improve medication delivery in Alzheimer's disease (AD) therapy.

REFERENCE:

1. Ling, Y**.,** Morgan, K., Kalsheker, N., 2003. Amyloid precursor protein (APP) and the biology of proteolytic processing: relevance to Alzheimer's disease. Int. J. Biochem. Cell Biol. 35, 1505–1535.
2. Sambamurti, K., Greig, N.H., Lahiri, D.K., 2002. Advances in the cellular and molecular biology of the beta-amyloid protein in Alzheimer's disease. Neuromolecular Med. 1, 1–31.
3. Kojro, E., Gimpl, G., Lammich, S., Marz, W., Fahrenholz, F., 2001. Low cholesterol stimulates the nonamyloidogenic pathway by its effect on the α-secretase ADAM 10. Proc. Natl. Acad. Sci. U.S.A. 98, 5815–5820.
4. Gabuzda, D., Busciglio, J., Yankner, B.A., 1993. Inhibition of beta-amyloid production by activation of protein kinase C. J. Neurochem. 61, 2326–2329.
5. Golde, T.E., Younkin, S.G., 2001. Presenilins as therapeutic targets for the treatment of Alzheimer's disease. Trends Mol. Med. 7, 264–269.
6. Dingwall, C., 2001. Spotlight on BACE: the secretases as targets for treatment in Alzheimer disease. J. Clin. Invest. 108, 1243–1246.
7. Howlett, D.R., Simmons, D.L., Dingwall, C., Christie, G., 2000. In search of an enzyme: the beta-secretase of Alzheimer's disease is an aspartic proteinase. Trends Neurosci. 23, 565– 570.
8. Vassar, R., 2001. The beta-secretase, BACE: a prime drug target for Alzheimer's disease. J. Mol.
9. Maiorini, A.F., Gaunt, M.J., Jacobsen, T.M., McKay, A.E., Waldman, L.D., Raffa, R.B., 2002. Potential novel targets for Alzheimer pharmacotherapy: I. Secretases. J. Clin. Pharm. Ther. 27, 169–183.
10. Citron, M., Westaway, D., Xia, W., Carlson, G., Diehl, T., Levesque, G., Johnson-Wood, K., Lee, M., Seubert, P., Davis, A., Kholodenko, D., Motter, R., Sherrington, R., Perry, B., Yao, H., Strome, R., Lieberburg, I., Rommens, J., Kim, S., Schenk, D., Fraser, P., St George Hyslop, P., Selkoe, D.J., 1997. Mutant presenilins of Alzheimer's disease increase production of 42-residue amyloid beta-protein in both transfected cells and transgenic mice. Nat. Med. 3, 67–72.
11. Duff, K., Eckman, C., Zehr, C., Yu, X., Prada, C.M., Perez-tur, J., Hutton, M., Buee, L., Harigaya, Y., Yager, D., Morgan, D., Gordon, M.N., Holcomb, L., Refolo, L., Zenk, B., Hardy, J., Younkin, S., 1996. Increased amyloid-beta42(43) in brains of mice expressing mutant presenilin 1. Nature 383, 710–713.
12. Scheuner, D., Eckman, C., Jensen, M., Song, X., Citron, M., Suzuki, N., Bird, T.D., Hardy, J., Hutton, M., Kukull, W., Larson, E., Levy-Lahad, E., Viitanen, M., Peskind, E., Poorkaj, P., Schellenberg, G., Tanzi, R., Wasco, W., Lannfelt, L., Selkoe, D., Younkin, S., 1996. Secreted amyloid beta-protein similar to that in the senile plaques of Alzheimer's disease is increased in vivo by the presenilin 1 and 2 and APP mutations linked to familial Alzheimer's disease. Nat. Med. 2, 864–870.
13. Schraen-Maschke, S., Dhaenens, C.-M., Delacourte, A., Sablonnière, B., 2004. Microtubule-associated protein tau gene: a risk factor in human neurodegenerative diseases. Neurobiol. Dis. 15, 449–460.
14. Hernández, F., Avila, J., 2008. The role of glycogen synthase kinase 3 in the early stages of Alzheimers' disease. FEBS Lett. 582, 3848–3854.
15. Braak, H., Braak, E., 1991. Neuropathologicalstageing of Alzheimer-related changes. ActaNeuropathol. 82, 239–259.
16. Farlow, M., 2002. A clinical overview of cholinesterase inhibitors in Alzheimer's disease. Int. Psychogeriatr. 14 Suppl 1, 93–126.
17. Salloway, S., Mintzer, J., Weiner, M.F., Cummings, J.L., 2008. Disease-modifying therapies in Alzheimer's disease. Alzheimers. Dement. 4, 65–79.
18. Costantino, H.R., Leonard, A.K., Brandt, G., Johnson, P.H., Quay, S.C., 2008. Intranasal administration of acetylcholinesterase inhibitors. BMC Neurosci. 9 Suppl3, S6.
19. Lou, G., Montgomery, P.R., Sitar, D.S., 1996. Bioavailability and pharmacokinetic disposition of tacrine in elderly patients with Alzheimer's disease. J. psychiatry Neurosci. 21, 334–339.
20. Gore, A. V, Liang, A.C., Chien, Y.W., 1998. Comparative biomembrane permeation of tacrine using Yucatan minipigs and domestic pigs as the animal model. J. Pharm. Sci. 87, 441–447.
21. Gowthamarajan, K., Jawahar, N., Wake, P., Jain, K., Sood, S., 2012. Development of buccal tablets for curcumin using Anacardiumoccidentale gum. Carbohydr. Polym. 88, 1177–1183.
22. Hamaguchi, T., Ono, K., Yamada, M., 2010. Curcumin and Alzheimer's disease. CNS Neurosci. Ther. 16, 285–297.
23. Modi, G., Pillay, V., Choonara, Y.E., Ndesendo, V.M.K., du Toit, L.C., Naidoo, D., 2009. Nanotechnological applications for the treatment of neurodegenerative disorders. Prog.Neurobiol. 88, 272–285.
24. Rahman, Z., Zidan, A.S., Khan, M. a, 2010. Non-destructive methods of characterization of risperidone solid lipid nanoparticles. Eur. J. Pharm. Biopharm. 76, 127–137.
25. Zhang, X., Liu, J., Qiao, H., Liu, H., Ni, J., Zhang, W., Shi, Y., 2010. Formulation optimization of dihydroartemisinin nanostructured lipid carrier using response surface methodology. Powder Technol. 197, 120–128.
26. Singare, D.S., Marella, S., Gowthamrajan, K., Kulkarni, G.T., Vooturi, R., Rao, P.S., 2010. Optimization of formulation and process variable of nanosuspension: An industrial perspective. Int. J. Pharm. 402, 213–220.
27. Freitas, C., Müller, R.H., 1999. Correlation between long-term stability of solid lipid nanoparticles (SLN) and crystallinity of the lipid phase. Eur. J. Pharm. Biopharm. 47, 125– 132.
28. Shafiq, S., Shakeel, F., Talegaonkar, S., Ahmad, F.J., Khar, R.K., Ali, M., 2007. Development and bioavailability assessment of ramiprilnanoemulsion formulation. Eur. J. Pharm. Biopharm. 66, 227–243.
29. Jain, K., Kumar, R.S., Sood, S., Dhyanandhan, G., 2013b. Betaxolol hydrochloride loaded chitosan nanoparticles for ocular delivery and their anti-glaucoma efficacy. Curr. Drug Deliv. 10, 493–499.
30. Jain, K., Kumar, R., Sood, S., Gowthamarajan, K., 2013a. Enhanced Oral Bioavailability of Atorvastatin via Oil-in-Water Nanoemulsion using Aqueous Titration Method. J. Pharm. Sci. Res. 5, 18–25.

31. Sood, S., Jawahar, N., Jain, K., Gowthamarajan, K., Meyyanathan, S.N., 2013. Olanzapine loaded cationic solid lipid nanoparticles for improved oral bioavailability. Curr. Nanosci. 9, 26–34.
32. Sood, S., Jawahar, N., Jain, K., Gowthamarajan, K., Meyyanathan, S.N., 2013. Olanzapine loaded cationic solid lipid nanoparticles for improved oral bioavailability. Curr. Nanosci. 9, 26–34
33. Costa, P., Lobo, J.M.S., 2001. Modeling and comparison of dissolution profiles. Eur. J. Pharm.Sci. 13, 123–133.
34. Seju, U., Kumar, A., Sawant, K.K., 2011. Development and evaluation of olanzapine-loaded PLGA nanoparticles for nose-to-brain delivery: in vitro and in vivo studies. ActaBiomater. 7, 4169–4176.
35. Costa, P., Lobo, J.M.S., 2001. Modeling and comparison of dissolution profiles. Eur. J. Pharm.Sci. 13, 123–133.
36.
37. Cavalli, R., Caputo, O., Eugenia, M., Trotta, M., Scarnecchia, C., Gasco, M.R., 1997. Sterilization and freeze-drying of drug-free and drug-loaded solid lipid nanoparticles. Int. J.Pharm. 148, 47–54.
38. Kovacevic, A., Savic, S., Vuleta, G., Müller, R.H., Keck, C.M., 2011. Polyhydroxy surfactants for the formulation of lipid nanoparticles (SLN and NLC): effects on size, physical stability and particle matrix structure. Int. J. Pharm. 406, 163–172.
39. Teeranachaideekul, V., Souto, E.B., Junyaprasert, V.B., Müller, R.H., 2007. Cetylpalmitate-based NLC for topical delivery of Coenzyme Q(10) - development, physicochemical characterization and in vitro release studies. Eur. J. Pharm. Biopharm. 67, 141–148.
40. Severino, P., Pinho, S.C., Souto, E.B., Santana, M.H. A., 2011. Polymorphism, crystallinity and hydrophilic-lipophilic balance of stearic acid and stearic acid-capric/caprylic triglyceride matrices for production of stable nanoparticles. Colloids Surf. B. Biointerfaces 86, 125–130.
41. Jenning, V., Thünemann, A.F., Gohla, S.H., 2000. Characterisation of a novel solid lipid nanoparticle carrier system based on binary mixtures of liquid and solid lipids. Int. J. Pharm. 199, 167–177.
42. Chen, H., Chang, X., Du, D., Liu, W., Liu, J., Weng, T., 2006. Podophyllotoxin-loaded solid lipid nanoparticles for epidermal targeting. J. Control. Release 110, 296–306.
43. Dai, W., Dong, L., S, L., Deng, Z., 2008. Combination of Pluronic/Vitamin E TPGS as a potential inhibitor of drug precipitation. Int. J. Pharm. 355, 31–37.
44. Ghosh, I., Bose, S., Vippagunta, R., Harmon, F., 2011. Nanosuspension for improving the bioavailability of a poorly soluble drug and screening of stabilizing agents to inhibit crystal growth. Int. J. Pharm. 409, 260–268
45. Hu, F., Jiang, S., Du, Y., Yuan, H., Ye, Y., Zeng, S., 2005. Preparation and characterization of stearic acid nanostructured lipid carriers by solvent diffusion method in an aqueous system. Colloids Surfaces B Biointerfaces 45, 167–173.
46. Mühlen, A., Mühlen, E., Niehus, H., Mehnert, W., 1996. Atomic force microscopy studies of solid lipid nanoparticles. Pharm. Res. 13, 1411–1416.